Peering into the Self-Assembly of Surfactant Templated Thin-Film Silica Mesophases

Dhaval A. Doshi,[†,⊥] Alain Gibaud,[‡,○] Valerie Goletto,[§] Mengcheng Lu,[†,#]
Henry Gerung,[†] Benjamin Ocko,[∥] Sang M. Han,[†] and C. Jeffrey Brinker*,[†,‡]

*Contribution from the Department of Chemical and Nuclear Engineering and Center for
Micro-Engineered Materials, University of New Mexico, Albuquerque, New Mexico 87131;
Sandia National Laboratories, Albuquerque, New Mexico 87106; Chimie de la Matière
Condensée, Université Pierre et Marie Curie, 75005 Paris, France; and Department of Physics,
Brookhaven National Laboratory, Upton, New York 11973*

Received December 2, 2002; E-mail: cjbrink@sandia.gov

Abstract: It is now recognized that self-assembly is a powerful synthetic approach to the fabrication of nanostructures with feature sizes smaller than achievable with state of the art lithography and with a complexity approaching that of biological systems. For example, recent research has shown that silica/surfactant self-assembly combined with evaporation (so-called evaporation induced self-assembly EISA) can direct the formation of porous and composite thin-film mesostructures characterized by precise periodic arrangements of inorganic and organic constituents on the 1–50-nm scale. Despite the potential utility of these films for a diverse range of applications such as sensors, membranes, catalysts, waveguides, lasers, nano-fluidic systems, and low dielectric constant (so-called low *k*) insulators, the mechanism of EISA is not yet completely understood. Here, using time-resolved grazing incidence small-angle X-ray scattering (GISAXS) combined with gravimetric analysis and infrared spectroscopy, we structurally and compositionally characterize in situ the evaporation induced self-assembly of a homogeneous silica/surfactant/solvent solution into a highly ordered surfactant-templated mesostructure. Using CTAB (cetyltrimethylammonium bromide) as the structure-directing surfactant, a two-dimensional (2-D) hexagonal thin-film mesophase (*p*6*mm*) with cylinder axes oriented parallel to the substrate surface forms from an incipient lamellar mesophase through a correlated micellar intermediate. Comparison with the corresponding CTAB/water/alcohol system (prepared without silica) shows that, for acidic conditions in which the siloxane condensation rate is minimized, the hydrophilic and nonvolatile silicic acid components replace water maintaining a fluidlike state that avoids kinetic barriers to self-assembly.

Introduction

Starting with homogeneous solutions of soluble silica (monomeric and oligomeric silicic acid species referred to generally as silicic acids) plus surfactant (and optionally other organic and inorganic ingredients) prepared in alcohol/water solvents, preferential evaporation of alcohol accompanying spin-coating,[2,3,10] dip-coating,[6,8,9,12,13] ink-jet printing,[18] aerosol deposi-

tion,[21] or selective dewetting[18] drives silica/surfactant self-assembly[1] into uniform or spatially patterned[18] thin-film mesophases. Through subsequent heating or exposure to catalysts or light,[9,22] these films can be processed into porous[2,3,6,8–10,12] or composite mesostructures[13,14] of potential utility for a diverse range of applications such as sensors,[15] membranes,[16] catalysts,

† University of New Mexico.
‡ Sandia National Laboratories.
§ Université Pierre et Marie Curie.
∥ Brookhaven National Laboratory.
⊥ Currently at Los Alamos National Laboratory, LANSCE-12, NM 87545, USA.
○ Université du Maine, Faculté des Sciences, UMR 6087, CNRS 72085, Le Mans Cedex 09, France.
Intel Corporation, Portland Technology Development, Hillsboro OR 97124, USA.

(1) Kresge, C. T., et al. Ordered Mesoporous Molecular-Sieves Synthesized By a Liquid-Crystal Template Mechanism. *Nature* **1992**, *359* (6397), 710–712.
(2) Brinker, C. J., et al. Evaporation-induced self-assembly: Nanostructures made easy. *Adv. Mater.* **1999**, *11* (7), 579–585.
(3) Ogawa, M. A Simple Set-Gel Route For the Preparation of Silica-Surfactant Mesostructured Materials. *Chem. Commun.* **1996**, (10), 1149–1150.
(4) Yang, H., et al. Free-standing and Oriented Mesoporous Silica Films Grown At the Air–Water Interface. *Nature* **1996**, *381* (6583), 589–592.
(5) Yang, H., et al. Synthesis of Oriented Films of Mesoporous Silica On Mica. *Nature* **1996**, *379* (6567), 703–705.
(6) Lu, Y. F., et al. Continuous Formation of Supported Cubic and Hexagonal Mesoporous Films By Sol–Gel Dip-Coating. *Nature* **1997**, *389* (6649), 364–368.
(7) Trau, M., et al. Microscopic Patterning of Orientated Mesoscopic Silica Through Guided Growth. *Nature* **1997**, *390* (6661), 674–676.
(8) Zhao, D., et al. Continuous Mesoporous Silica Films With Highly Ordered Large-Pore Structures. *Adv. Mater.* **1998**, *10* (16), 1380–1385.
(9) Doshi, D. A., et al. Optically, defined multifunctional patterning of photosensitive thin-film silica mesophases. *Science* **2000**, *290* (5489), 107–111.
(10) Besson, S., et al. A new 3D organization of mesopores in oriented CTAB silica films. *J. Phys. Chem. B* **2000**, *104* (51), 12095–12097.
(11) Yao, N., et al. Disorder–order transition in mesoscopic silica thin films. *Chem. Mater.* **2000**, *12* (6), 1536–1548.
(12) Grosso, D., et al. Highly oriented 3D-hexagonal silica thin films produced with cetyltrimethylammonium bromide. *J. Mater. Chem.* **2000**, *10* (9), 2085–2089.
(13) Sellinger, A., et al. Continuous Self-Assembly of Organic–Inorganic Nanocomposite Coatings That Mimic Nacre. *Nature* **1998**, *394* (6690), 256–260.

waveguides,[17] lasers,[17] nano-fluidic systems,[18] and low dielectric constant (so-called low *k*) insulators.[19,20] This evaporation-induced self-assembly (EISA) process[2] is useful because it enables rapid, efficient integration of well-defined nanostructures into microelectronic devices and microsystems, using readily available processing methods. However, understanding and ultimately control of self-assembly is a critical need for its emergence from largely a laboratory practice to a reliable "tool" for nanofabrication.

Recent spatially resolved spectroscopic studies[6,23,24] and time resolved[25−27] and spatially resolved X-ray scattering[28] experiments have established the critical micelle concentration and have observed the transient formation of thin-film mesophases during EISA. In situ X-ray scattering measurements performed to date have employed (i) non-steady-state coating conditions[25−27] in which the film is draining and evaporating or (ii) steady-state dip coating conditions,[28] but both have relied on optical interferometry,[25−28] which is limited in resolution to $\sim\lambda/2$ (where λ is the wavelength of the monochromatic light source) to monitor film thickness. The non-steady-state conditions[26,29] do not allow determination of composition from the observed film thickness and therefore have not correlated mesostructure formation with compositional variations. For the steady-state dip-coating conditions, calculation of compositional changes occurring near and beyond the "drying line", where mesophase formation and transformations have been observed,[28] is precluded by the limited resolution of optical interferometry. Thus for evaporating systems, it has not yet been possible to make valid comparisons with the phase behavior of bulk surfactant/water/alcohol systems necessary to establish how silica and the presence of interfaces influence the self-assembly pathway.

To derive structural and compositional information *simultaneously*, our approach employs time-resolved in situ grazing
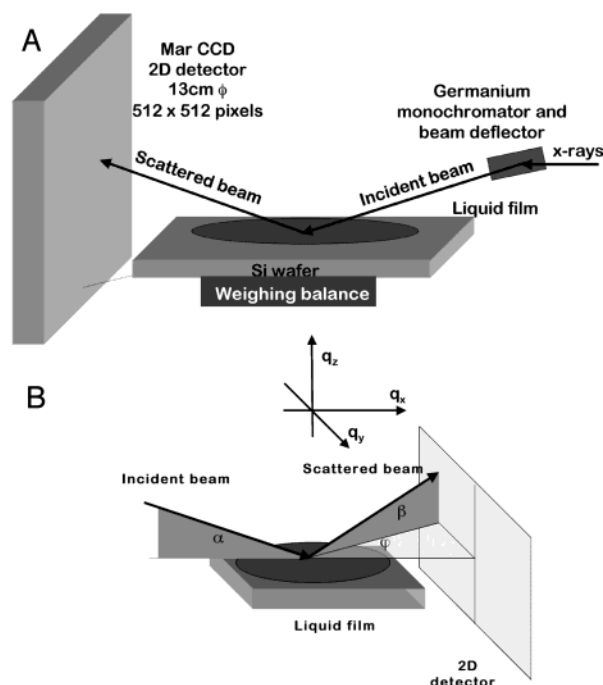

Figure 1. Experimental setup and reciprocal space schematics. (A) The liquid spectrometer setup used for GISAXS experiments. (B) Schematic of the reciprocal space probed by the experiment, where α is the angle of incidence, β is the scattering angle in the specular direction, and φ is the scattering angle in plane. The reciprocal lattice is defined by q_z, normal to the substrate surface. q_x and q_y are the in-plane directions.

incidence small-angle X-ray scattering (GISAXS), using a high brilliance synchrotron source (X22B, National Synchrotron Light Source, Brookhaven National Laboratory), combined with gravimetric analysis to study self-assembly of a slowly evaporating film maintained in a horizontal geometry under controlled environmental conditions (see Experimental Section and Figure 1). For the cationic surfactant CTAB, three CTAB/silica/ethanol/water systems prepared under acidic conditions with differing CTAB/Si molar ratios (0.10, 0.12, 0.16) were studied along with a solution prepared like sample 0.12 but without silica (sample, WS; see Experimental Section). In situ stress and attenuated total reflection-Fourier transform infrared spectroscopy (ATR-FTIR) measurements performed using the identical horizontal geometry combined with X-ray reflectivity analysis of the final self-assembled films enabled further structural interpretation of the GISAXS results, providing greater insight into the self-assembly pathway. Comparisons with other surfactant templated systems that yield lamellar and cubic mesophases allow a generalized view of the self-assembly process.

Experimental Section

GISAXS. Sols were prepared using a two-step procedure. First, a mixture of TEOS ($Si(OC_2H_5OH)_4$), ethanol, water, and HCl (mole ratios $1:3:1:5 \times 10^{-5}$) was refluxed at 80 °C for 60 min. Additional, ethanol, acid, and surfactant were added to obtain final sols with the following molar ratios: 1 TEOS:20 C_2H_5OH:5.4 H_2O:0.004 HCl:$0.10−0.16$ CTAB, 1 TEOS:20 C_2H_5OH:5.4 H_2O:0.004 HCl:0.05 SDS, or 1 TEOS:20 C_2H_5OH:5.1 H_2O:0.074 HCl:0.085 Brij-56, where the acid concentration was chosen to minimize the siloxane condensation rate thereby promoting EISA. Solutions (initial weight $m_o = 0.13−0.15$ g, which, assuming uniform wetting of the substrate and complete solvent evaporation, correspond to a final thickness of 20 μm) were dispensed onto a silicon (100) substrate positioned horizontally on the platform

(14) Lu, Y. F., et al. Self-assembly of mesoscopically ordered chromatic polydiacetylene/silica nanocomposites. *Nature* **2001**, *410* (6831), 913−917.
(15) Domansky, K., et al. Chemical sensors based on dielectric response of functionalized mesoporous silica films. *J. Mater. Res.* **2001**, *16* (10), 2810−2816.
(16) Tsai, C. Y., et al. Dual-layer asymmetric microporous silica membranes. *J. Membr. Sci.* **2000**, *169* (2), 255−268.
(17) Yang, P. D., et al. Mirrorless lasing from mesostructured waveguides patterned by soft lithography. *Science* **2000**, *287* (5452), 465−467.
(18) Fan, H. Y., et al. Rapid prototyping of patterned functional nanostructures. *Nature* **2000**, *405* (6782), 56−60.
(19) Miller, R. D. Device physics: In search of low-k dielectrics. *Science* **1999**, *286* (5439), 421−423.
(20) Fan, H. Y., et al. Self-assembled aerogellike low dielectric constant films. *J. Non-Cryst. Solids* **2001**, *285* (1−3), 79−83.
(21) Lu, Y. F., et al. Aerosol-assisted self-assembly of mesostructured spherical nanoparticles. *Nature* **1999**, *398* (6724), 223−226.
(22) Clark, T., et al. A new application of UV-ozone treatment in the preparation of substrate-supported, mesoporous thin films. *Chem. Mater.* **2000**, *12* (12), 3879−3884.
(23) Huang, M. H., et al. In situ probing by fluorescence spectroscopy of the formation of continuous highly ordered lamellar-phase mesostructured thin films. *Langmuir* **1998**, *14* (26), 7331−7333.
(24) Huang, M. H.; Dunn, B. S.; Zink, J. I. In situ luminescence probing of the chemical and structural changes during formation of dip-coated lamellar phase sodium dodecyl sulfate sol−gel thin films. *J. Am. Chem. Soc.* **2000**, *122* (15), 3739−3745.
(25) Grosso, D., et al. Two-dimensional hexagonal mesoporous silica thin films prepared from black copolymers: Detailed characterization amd formation mechanism. *Chem. Mater.* **2001**, *13* (5), 1848−1856.
(26) Grosso, D., et al. An in situ study of mesostructured CTAB−silica film formation during dip coating using time-resolved SAXS and interferometry measurements. *Chem. Mater.* **2002**, *14* (2), 931−939.
(27) Grosso, D., et al. Phase transformation during cubic mesostructured silica film formation. *Chem. Commun.* **2002** (7), 748−749.
(28) Doshi, D. A., et al. In situ X-ray scattering study of continuous silica−surfactant self-assembly during dip coating. *J. Phys. Chem. B* **2003**, web published at www.acs.org.
(29) Grosso, D., et al. Two-dimensional hexagonal mesoporous silica thin films prepared from block copolymers: Detailed characterization and formation mechanism. *Chem. Mater.* **2001**, *13* (5), 1848−1856.

of a weighing balance confined within a cell, allowing controlled solvent evaporation. Use of a liquid spectrometer permitted X-rays ($\lambda = 1.5826$ Å), deflected by a Ge monochromator, to impinge upon the surface of the liquid film at a controlled angle of incidence (0.35°), while maintaining the film in a horizontal configuration (see Figure 1). The scattering was monitored with an MAR CCD 2D detector, and the frames, 512×512 pixels, were continuously collected every 15 s with an acquisition time of 10 s and a transfer time of 5 s. An He filled beam pipe was placed in front of the 2D detector, located 47 cm from the sample, to reduce air scattering/absorption.

X-ray Reflectivity. X-ray reflectivity measurements were performed at the X22A beam line, National Synchrotron Light Source, Brookhaven National Laboratory, USA, with an 11 keV monochromatic beam. The incident and scattered beams were collimated so as to achieve a direct beam fwhm (full width at half-maximum) of 0.04°. Measurements were made under strictly specular conditions and corrected by subtracting the longitudinal specular background that was found to be almost negligible (3 orders of magnitude lower). The thin-film sample was spin-coated using a sol aged to enhance the extent of siloxane condensation in order to kinetically impede self-assembly and was further diluted with ethanol (1 TEOS:115 C_2H_5OH:5 H_2O:0.005 HCl: 0.10 CTAB) to obtain <1000 Å film thickness.

Cantilever Beam Measurements. In situ stress measurements were performed in a custom built setup.[30] Sol (20 μL) was dispensed onto a double side polished 150-μm thick Si wafer that was fixed at one end and hence served as a horizontal cantilever. The free end deflection (δ) of the cantilever was monitored by a laser beam/photodetector setup and related to the average biaxial stress (σ) in the film by Stoney's equation: $\sigma = (Ed^2\delta)/(3L^2(1 - \upsilon)t)$; where E is the Young's modulus of the substrate, d, the substrate thickness, L, the cantilever length, υ, Poisson's ratio for the substrate, and t, the film thickness.

ATR-FTIR Spectroscopy. In situ ATR-FTIR experiments were performed on a Nexus 670 spectrometer manufactured by Nicolet, using a trapezoidal Ge (111)-oriented ATR crystal $50 \times 10 \times 2$ mm³ in size. The crystal was cleaned by immersing it in HF solution (10 wt %) followed by acetone. A controlled amount of sol (50 μL) was then added to the top surface of the crystal. The beam from the spectrometer enters at normal incidence into the bevelled side of the crystal, undergoes multiple reflections (~24 on both top and bottom surfaces), and comes out at the other bevelled end. The outcoming IR signal is focused via a KBr lens onto an HgCdTe IR detector. Spectra from 650 to 4000 cm⁻¹ (wavenumbers) were collected with a resolution of 2 cm⁻¹. Each spectrum is an average of 20 scans that take 14 s to be acquired at a scan speed of 5.7 cm/s followed by a delay of 1 s between spectra.

Results and Discussion

Figure 2 shows the temporal evolution of percentage starting weight for the 0.12 sample along with that calculated for the surfactant, CTAB. Based on the initial composition (Figure 2) and the high vapor pressure (~60 Torr) of ethanol at 25 °C compared to that of water (~24 Torr), we attribute the initial ($t < 600$ s) rapid weight loss to evaporation of ethanol. Beyond ~600 s, the evaporation rate decreases dramatically, and the remaining weight loss (~2 wt %) is consistent with that of water. The self-assembly pathway comprises four successive stages, (I) isotropic, (II) lamellar, (III) correlated micellar, and (IV) hexagonal (Figures 2 and 3), each characterized qualitatively by their respective GISAXS patterns (Figure 4).

Figure 3 plots the d-spacing observed normal to the substrate (viz. the bilayer d-spacing for lamellar or d_{cm} for correlated

(30) Lu, M.; Brinker, C. J. Stress Development in Low Dielectric Constant Silica Films during Drying and Heating Process. *Mater. Res. Soc. Symp. Proc.* **1999**.
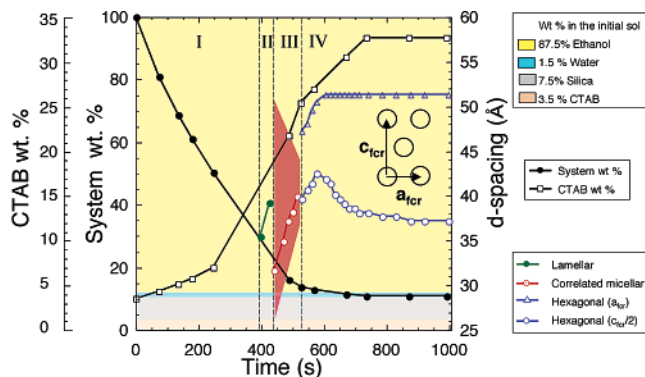
Figure 2. Temporal evolution of structure and composition for the 0.12 sample: (I) the isotropic phase, $t = 246$ s; (II) the lamellar phase, $t = 396$ s, $d = 35.4$ Å, $t = 426$ s, $d = 39.2$ Å; (III) correlated micellar phase, $t = 441$ s, 26.2 Å $< d = 31.7$ Å < 51 Å, $t = 526$ s, 37 Å $< d = 40$ Å < 44 Å; (IV) hexagonal mesophase, $t = 541$ s, $c_{fcr}/2 = 39.7$ Å, $a_{fcr} = 47.2$ Å, at $t = 616$ s, with siloxane condensation causing one-dimensional shrinkage normal to the substrate $c_{fcr}/2 = 41.9$ Å, $a_{fcr} = 51.3$ Å, $t = 996$ s, $c_{fcr}/2 = 37.2$ Å, $a_{fcr} = 51.3$ Å.

micellar or $c_{fcr}/2$ for hexagonal) and, for the hexagonal mesophase, the in-plane spacing a_{fcr} (fcr is the face-centered rectangular lattice representation of the hexagonal lattice with $c_{fcr}/a_{fcr} = \sqrt{3}$). ((I) the isotropic phase, $t = 246$ s; (II) the lamellar phase, $t = 396$ s, $d = 35.4$ Å, $t = 426$ s, $d = 39.2$ Å; (III) the correlated micellar phase, $t = 441$ s, 26.2 Å $< d = 31.7$ Å < 51 Å, $t = 526$ s, 37 Å $< d = 40$ Å < 44 Å; (IV) the hexagonal mesophase, $t = 541$ s, $c_{fcr}/2 = 39.7$ Å, $a_{fcr} = 47.2$ Å, at $t = 616$ s; siloxane condensation causes one-dimensional shrinkage normal to the substrate $c_{fcr}/2 = 41.9$ Å, $a_{fcr} = 51.3$ Å, $t = 996$ s, $c_{fcr}/2 = 37.2$ Å, $a_{fcr} = 51.3$ Å.) As discussed below, within each of the stages II−IV, we observe increases in the respective d-spacings due to the continually evolving system composition. Figure 3 maps the evaporation-induced compositional trajectories of the three CTAB/silica systems (derived from Figure 2 and equivalent data obtained for the 0.10 and 0.16 systems) onto the bulk water/ethanol/CTAB phase diagram,[31] considering the hydrophilic silicic acid precursors to be equivalent to water. Also plotted is the trajectory for sample WS. The regions I, H, and C correspond to the isotropic, hexagonal, and crystalline CTAB phases reported in the bulk water/ethanol/CTAB system by Fontell et al.[31] Selected corresponding GISAXS patterns obtained after the specified times, t (seconds), are presented in Figures 4 and 5.

At time $t < 396$ s, the GISAXS patterns show no diffraction peaks (Figure 4a) indicative of an isotropic phase. The intense line of scattering in the z-direction is a specular streak attributed to diffuse scattering arising from capillary waves present at the fluid, liquid−air interface. Although we surpass the critical micelle concentration, cmc at $t = 246$ s and $w_{CTAB} = 7\%$, based on a previous molecular probe study[6] conducted during EISA, no periodic, ordered structures develop, consistent with expectations from the bulk CTAB/ethanol/water phase diagram (Figure 3).

The sudden appearance of a single Bragg spot in the direction normal to the substrate surface at $t = 396$ s (Figure 4, panel b) marks the beginning of the lamellar stage (396 s $< t <$ 441 s). The Bragg spot is first observed at $q_z = 0.178$ Å⁻¹, correspond-

(31) Fontell, K., et al. Phase-Equilibria and Structures in Ternary-Systems of a Cationic Surfactant (C16tabr or (C16ta)2so4), Alcohol, and Water. *Colloid Polym. Sci.* **1991**, *269* (7), 727−742.
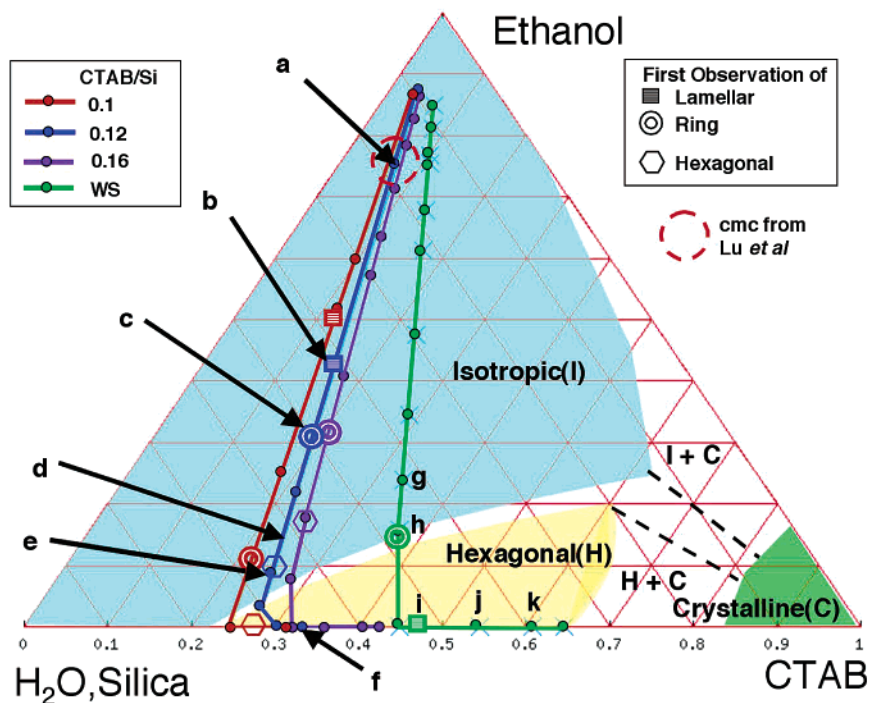
Figure 3. Bulk and thin-film ternary phase diagram. The evaporation-induced compositional trajectories of the three CTAB/silica systems (0.10, 0.12, and 0.16) and the WS system are mapped onto the bulk water/ethanol/CTAB phase diagram, considering the hydrophilic silicic acid precursors to be equivalent to water.
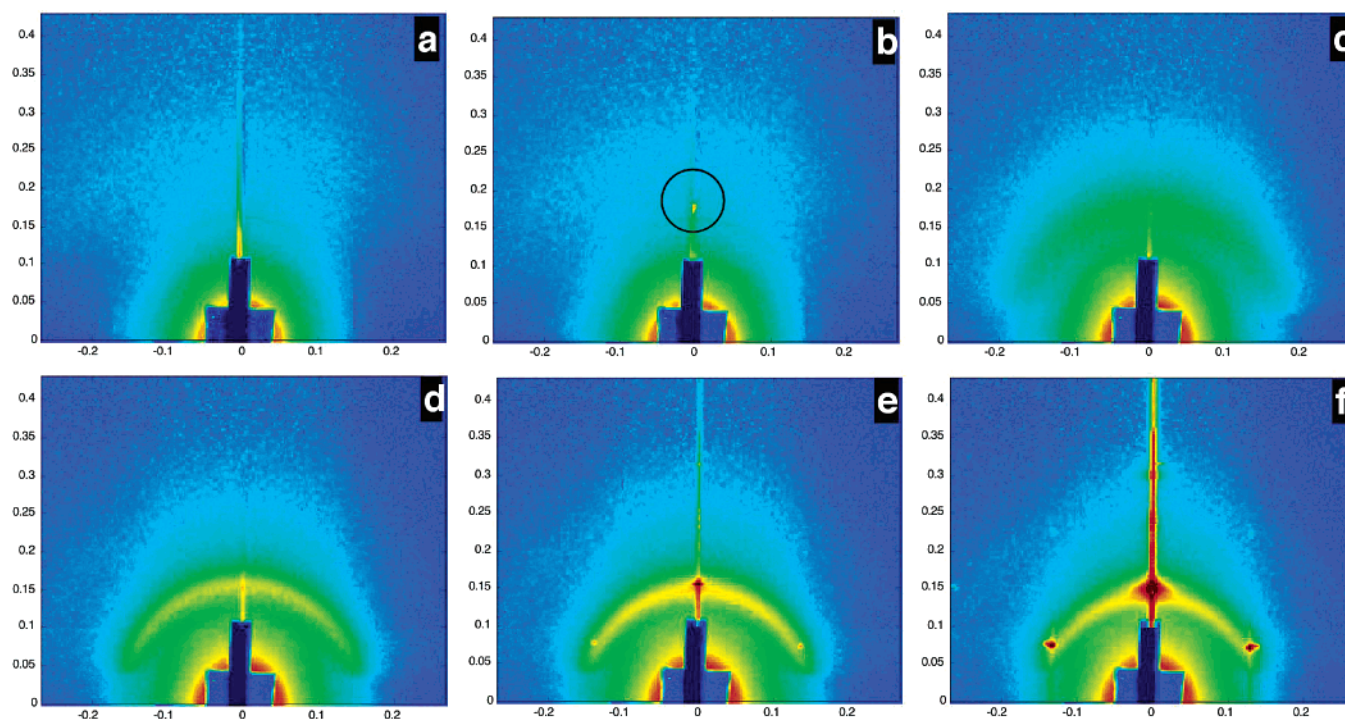

Figure 4. GISAXS patterns obtained after the specified times, *t* (seconds), are presented for sample 0.12, corresponding to the following: (a) the isotropic phase, (b) the lamellar mesophase, (c and d) the correlated micellar, and (e and f) the hexagonal mesophase.

ing to $d = 35.4$ Å, but with continuing evaporation of ethanol, the d-spacing increases to 39.2 Å. The absence of any peaks in q_y, combined with the spot orientation, and d-spacing are a clear signature of smectic ordering parallel to the substrate surface. From the peak width (0.007 Å^{-1}), we calculate a domain size of 895 Å,[32] corresponding to approximately 25 lamellae oriented parallel to the substrate surface. The formation of an incipient

lamellar mesophase at an average $w_{CTAB} = 16.5$ wt % is completely unexpected from the bulk phase diagram (Figure 3) and is not observed in the WS system (see Figure 5, panel g). Based on orientation, we attribute its appearance to an interfacial effect (not accounted for in the bulk phase diagram).

(32) Warren, B. E. *X-ray Diffraction*; Dover Publications Inc.: 1990.
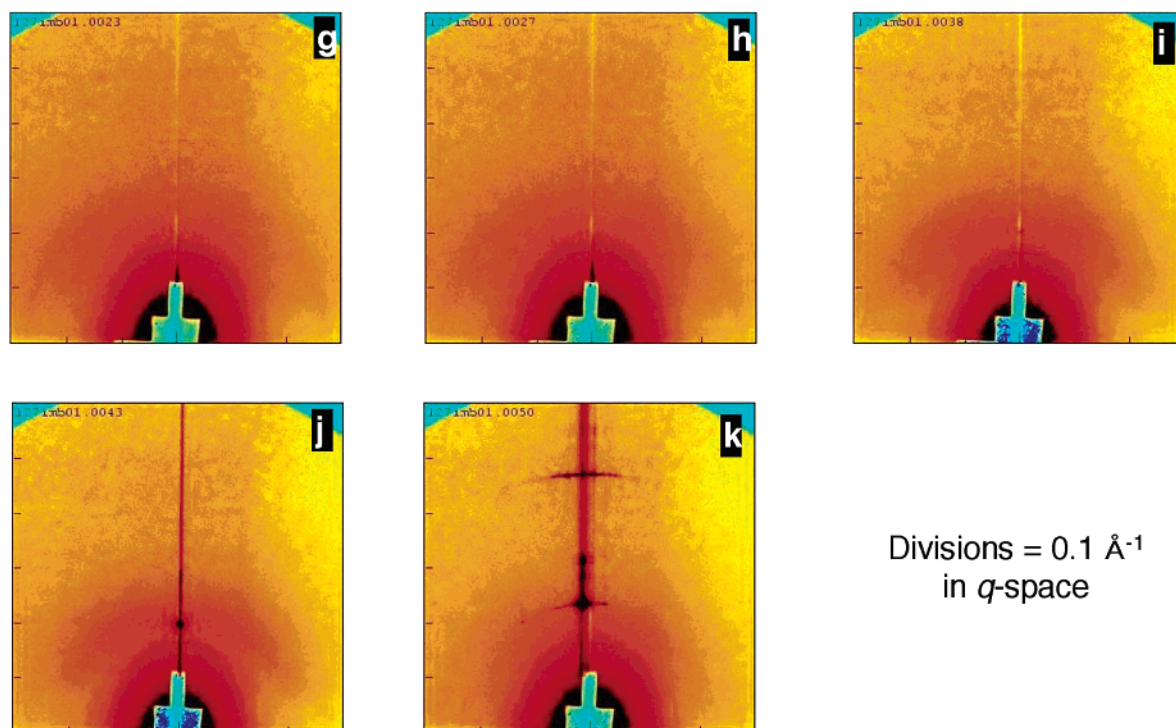
Figure 5. GISAXS patterns obtained after the specified times, t (seconds) for the WS sample, corresponding to the following: (g) isotropic, (h) correlated micellar, (i and j) lamellar and correlated micellar, and (k) crystalline CTAB.

In that Monte Carlo modeling studies of surfactant self-assembly have not predicted a bulk or interfacially organized lamellar mesophase in this (ethanol-rich) compositional range,[33] and the measured lamellar d-spacing is comparable to those of CTAB/water ($d = 35$ Å)[34] or CTAB/silica ($d = 34.5$ Å)[6] systems, we must conclude that the incipient lamellar mesophase is largely depleted of ethanol and requires silicic acid for its formation. Conceivably rapid ethanol evaporation from the liquid–vapor interface locally enriches surface regions in CTAB, silica, and water to the extent that an incipient hydrogen-bonded CTAB/silica lamellar mesophase develops that inhibits further ethanol diffusion within it, thereby temporarily stabilizing it. Because the overall evaporation rate appears unaffected (Figure 2), we surmise that the lamellar regions are not continuous but rather confined to islands between which ethanol freely evaporates. (In a permeation study of a lamellar composite prepared by EISA,[13] we determined the coherence length of the lamellae to be on the order of only 55 nm.) Lateral wetting then maintains a uniform ethanol surface concentration, which governs the mass transfer coefficient and allows ethanol evaporation to proceed at a nearly constant rate (see Figure 2).

At $t = 441$ s, the disappearance of the lamellar diffraction spot and concomitant appearance of a broad, diffuse arc at larger q (than that of the disappearing spot, Figure 4, panel c) signifies the beginning of the correlated micellar stage, attributed to spherical or cylindrical micelles exhibiting some degree of spatial registry. Throughout this stage, the scattering intensifies, the width of the arc decreases, and the characteristic center-to-

center spacing (d_{cm}) of the scattering species, proportional to the inverse arc radius, increases (Figure 2 and Figure 4, panels c and d). The presence of the arc and its increasing intensity and narrowing width are attributed to an enhanced spatial correlation of micelles resulting from their increasing number density (due to the progressive depletion of ethanol) and conceivably from their positioning by regular undulations of the lamellar mesophase. The angular continuity of the arc indicates absence of any 2D periodicity. Experimental conditions prevent determination of the form factor, so we cannot distinguish between spherical and cylindrical micelles; however, at the end of this stage, the angular extension of the arc of highest scattering intensity (attributable to the predominant scattering species) is limited in q-space to the boundary defined by the Bragg spots from the ensuing hexagonal phase. Thus we suppose the correlated micellar stage to involve the transformation of spherical to wormlike cylindrical micelles and their prepositioning into a highly correlated proto-hexagonal arrangement. The correlated micellar structure first appears in the homogeneous portion of the phase diagram (Figure 3), and comparison with samples 0.10 and 0.16 indicates a dependence on wt % CTAB, in all three samples its first appearance occurring near 19 wt % CTAB. For the WS sample, evidence of a correlated phase is not observed until the CTAB concentration is increased to ~38% at the boundary of the hexagonal phase field (Figure 2 and Figure 5, panel h). The different behaviors of samples prepared with and without silica again illustrate that the silicic acid species actively participate in the self-assembly process.

At $t = 531$ s, the sudden appearance of three well-defined Bragg spots positioned along the high q boundary of the arc, $q_r = 0.158$ Å^{-1}, (defining adjacent 60° central angles with respect to the origin, Figure 4, panel e) indicates the emergence of a

(33) Rankin, S. E.; Malanoski, A.; van Swol, F. Monte Carlo Simulation of Amphiphile Self-Assembly during Dip Coating. *Mater. Res. Soc. Symp. Proc.* **2001**.

(34) Auvray, X., et al. X-ray Diffraction Study of Mesophases of Cetyltrimethylammonium Bromide in Water, Formamide, and Glycerol. *J. Phy. Chem.* **1989**, *93* (21), 7458–7464.
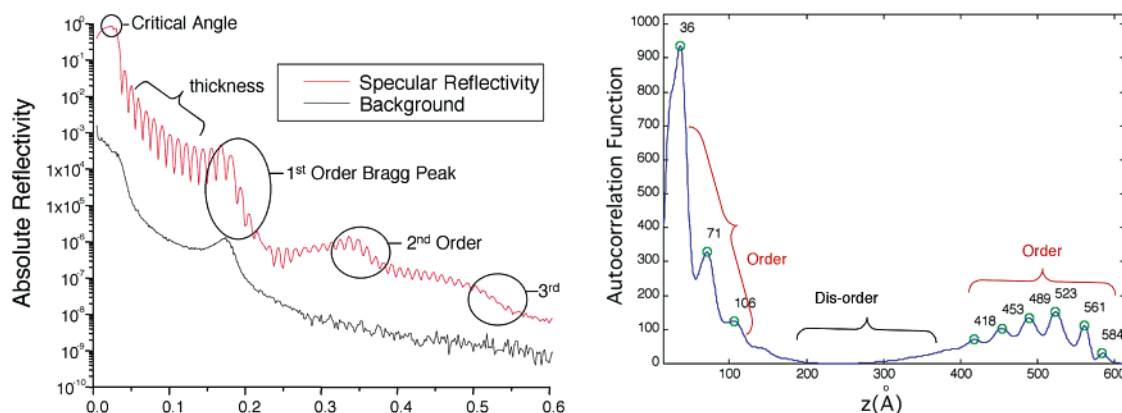
Figure 6. Evidence for interfacial growth of the mesostructure determined by X-ray reflectivity. (A) The specular reflectivity plot. (B) An autocorrelation function of the X-ray reflectivity curve with peaks labeled by their z-values.

hexagonal mesophase (space group $p6mm$) with tube axes oriented parallel to the substrate surface in an AB stacking configuration. The hexagonal phase is defined by a hexagonal lattice parameter, $a_{hex} = 47.2$ Å, or equivalently by face-centered rectangular lattice parameters $a_{fcr} = 47.2$ Å and $c_{fcr} = 79.4$ Å (with $c_{fcr}/a_{fcr} = \sqrt{3}$) (see Figure 3). Comparison of the three CTAB/Si samples shows the appearance of the hexagonal mesophase to follow the contour of the hexagonal phase boundary in the phase diagram (Figure 3). The WS sample, however, shows no evidence of a hexagonal mesophase, forming a lamellar mesophase followed by CTAB crystallization (Figure 5, panels j and k).

The coexistence of the correlated cylindrical micellar and hexagonal mesophases (diffraction spots superimposed on the arc of intensity in Figure 4, panels e and f) provides evidence for a first-order, disorder-to-order phase transformation.[11] X-ray reflectivity data for the 0.1 sample kinetically trapped (solidified) during this phase transformation are shown in Figure 6. The specular reflectivity plot exhibits Kessig fringes arising from the film thickness (~ 586 Å) and the first-, second-, and third-order Bragg peaks corresponding to a d-spacing of 37.3 Å. Figure 6B shows an autocorrelation function of the X-ray reflectivity curve resulting from periodic variations in the derivative of the electron density profile in the z-direction (normal to the substrate surface).[35] The presence of peaks at the high and low values of z and their absence at intermediate values indicate the existence of a disordered region sandwiched by ordered regions at the interfaces. The GISAXS pattern (Figure 7) of this film shows a ring superimposed on a hexagonal arrangement of spots consistent with the presence of ordered and disordered regions in the film. The symmetrical nature of the autocorrelation function precludes us from identifying the substrate−film versus the film−air interface, but these results confirm that the transformation occurs by growth of the interfacially organized hexagonal mesophase inward from both the original liquid−vapor and solid−liquid interfaces (Figure 6B) as originally postulated by Lu et al.[6] (for CTAB) and subsequently by Grosso et al.[25] for a block copolymer templated film. Cross-sectional TEM of a calcined film (Figure 8) prepared to freeze-in the structure during the disorder-to-order phase transformation shows an interfacially aligned hexagonal mesophase at the top and bottom interfaces and an intervening
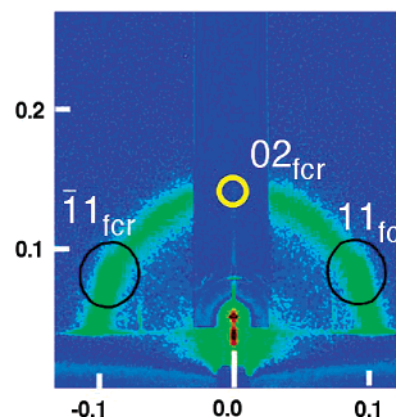
(35) Gibaud, A. *X-ray and neutron reflectivity: principles and applications*; Daillant, J., Gibaud, A., Eds.; Springer: 1999; Vol. m58, pp 87−120.

Figure 7. GISAXS pattern of the film. Attenuation of scattering in the specular direction in the vicinity of the critical angle used to prevent detector saturation masks the 02_{fcr} diffraction spot.

wormlike micellar mesostructure, confirming the interpretation of the reflectivity results.

Figure 9 shows a sequence of GISAXS patterns for anionic (sodium dodecyl sulfate SDS) and nonionic (Brij-56 (CH$_3$-(CH$_2$)$_{15}$(CH$_2$CH$_2$O)$_9$CH$_2$CH$_2$OH)) surfactant systems known to form lamellar[23,24] and cubic[8] surfactant/silica mesophases, respectively. The film prepared from a homogeneous solution containing the anionic surfactant SDS exhibits an interfacially aligned lamellar phase. At $t = 570$ s, $w_{SDS} = 5\%$, $m = 0.23m_o$, the 003 lamellar reflection observed at $q_z = 0.49$ Å^{-1}, corresponds to $c_{lam} = 38.5$ Å (Figure 9a1). At $t = 585$ s, $w_{SDS} = 5.8\%$, $m = 0.20m_o$, the 002 and 003 reflections are observed (see Figure 9a2), and at $t = 630$ s, $w_{SDS} = 6.5\%$, $m = 0.18m_o$, the 001, 002, and 003 reflections are observed (Figure 9a3). The progressive appearance of additional diffraction spots indicates a continuing increase in the extent of order.

The film prepared with Brij-56 (B56) evolves from an isotropic solution to a correlated micellar intermediate as evinced by the ring in Figure 9b1 at $t = 300$ s, $w_{B56} = 23\%$, $m = 0.20m_o$ (often proceeded by an incipient lamellar mesostructure). The correlated micellar phase transforms into a hexagonal mesophase at $t = 330$ s ($w_{B56} = 28\%$, $m = 0.16m_o$ with $a_{fcr} = 62.1$ Å, $c_{fcr} = 104.5$ Å in Figure 9b2) that further transforms, presumably due to a condensation driven phase transformation,[9] to a cubic mesophase at $t = 670$ s ($w_{B56} = 34\%$, $m = 0.14m_o$), as is evident from the array of spots indexed in Figure 9b3. The cubic mesophase exhibits several conserved reflections with the
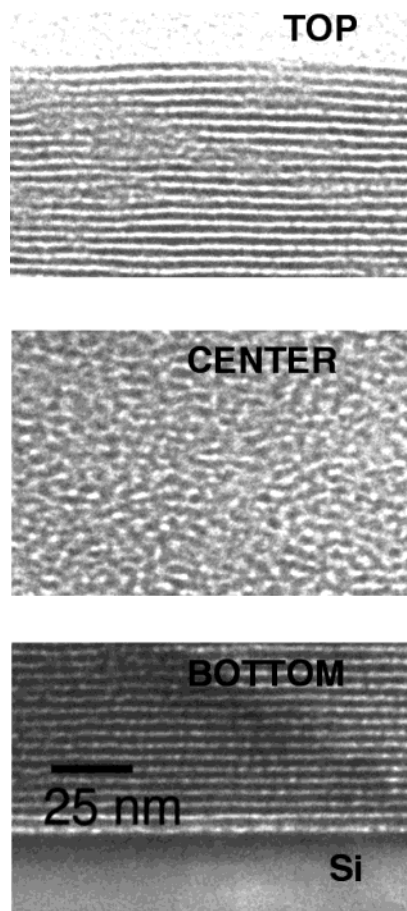
Figure 8. Cross-sectional TEM of a calcined film prepared to freeze-in the structure during the disorder-to-order phase transformation.

hexagonal phase and is consistent with a primitive cubic lattice with $a = 125.1$ Å. Figure 9b3 inset shows a TEM image of the [100] orientation of the cubic mesophase.

For all three systems (CTAB, SDS, and Brij-56), we find that the presence or absence of hydrophilic silica species dramatically influences mesophase development. Generally without silica, evaporation of solutions such as WS and others, where the amount of silica removed is compensated for by an equivalent amount of water, results in a crystalline surfactant product without forming the mesophase(s) anticipated from the bulk phase diagram. This apparent kinetic effect presumably results from the evaporation of water. We suppose that such kinetic barriers are avoided for silica containing systems because the silicic acid species undergo limited siloxane condensation and serve as nonvolatile fluids as hydrophilic as water (see further discussion below concerning stress development).

Re-examination of Figure 2 shows that in each of regions II−IV loss of ethanol is accompanied by an increase in the corresponding d-spacing of the lamellar, correlated micellar, and hexagonal mesophases, respectively. We attribute this behavior to a continuing reorganization of the surfactants within the lamellar or micellar structures due to ethanol evaporation. Monte Carlo simulations of lamellar mesophases in bulk ethanol/water/surfactant systems show ethanol molecules to be located adjacent to the surfactant headgroups with their hydrocarbon tails oriented toward the hydrophobic micellar core.[28] This arrangement promotes surfactant tail interdigitation in the lamellar mesophase due to favorable hydrophobic interactions.[28] Evaporation of

ethanol results in an unfavorable interaction between the hydrophobic surfactant tails and the hydrophilic water/silica-rich solvent, causing the bilayer spacing to increase (extent of inter-digitation decreases) as we observed for both the silica-containing and WS samples. Similarly, within cylindrical micelles, ethanol evaporation causes the surfactant tails to rearrange to become more radially oriented with respect to the cylinder axis. This causes an expansion of the micelle diameter (manifested as an increase in d_{cm} for the correlated micellar phase, Figure 2, region III, and an increase in a_{fcr} and c_{fcr} for the hexagonal mesophase, Figure 2, region IV) up until about 600 s, where ethanol evaporation is complete. (Details of this phenomena are published in ref 28.) Micellar expansion with reducing ethanol concentration was also observed in the bulk ethanol/water/CTAB system.[31] Comparison of the systems, 0.10, 0.12, 0.16, shows the percent expansion in the hexagonal unit cell dimension, a_{fcr}, observed in region IV to be directly proportional to the amount of ethanol present when the hexagonal phase first formed (see Table 1 and Figure 3).

Our observation of a continuous reorganization of both mesostructure and lattice dimension within regions II−IV emphasizes the need to suppress the siloxane condensation rate to allow self-assembly to proceed unimpeded. This is ac-complished in our experiments by using an initial HCl concen-tration of $\sim 10^{-2}$ M. Cantilever beam stress measurements recorded in the same horizontal configuration show that, for this acid-catalyzed sol, biaxial tensile stress, attributable to capillary stress and/or network condensation, normally observed during sol−gel film deposition[36] develops very slowly for the film prepared without surfactant and is almost completely suppressed within the first 10 min for the 0.16 film prepared with surfactant (Figure 10). Beyond 10 min, the 0.16 film develops a low level of stress and we observe a reduction in the hexagonal d-spacing c_{fcr} in the GISAXS experiment (Figure 3). Because the templated films are nonporous and therefore develop no capillary stress, the stress and reduction in d-spacing observed for the 0.16 film are attributed to the onset of siloxane condensation and accompanying, constrained, one-dimensional shrinkage normal to the substrate surface. The dramatic differ-ences in stress observed for the films prepared with and without surfactant is due largely to the development of capillary stress in the film prepared without surfactant, which, upon drying, is observed to be microporous.[16] However, we suspect that electrostatic and hydrogen-bonding interactions between the silanol moieties and the hydrophilic surfactant headgroups could serve to protect and orient the reactive silanols so as to further suppress their rates of siloxane condensation. Suppression of the siloxane condensation rate for surfactant-templated silicates prepared near pH 2 is well established from (i) self-assembly confined within liquid (aerosol) droplets in which the mesos-tructure continually rearranges in response to loss of solvent,[21] (ii) reversible effects of humidity on the structure of thin-film mesophases,[37] and (iii) photopatterning of photosensitive thin-film mesophases[9]

Figure 11 plots selected time-resolved ATR-FTIR spectra acquired in situ during evaporation for the 0.16 CTAB sample

(36) Cairncross, R. A., et al. Pore evolution and solvent transport during drying of gelled sol−gel coatings: Predicting "Springback". *Drying Technol.* **1997**, *15* (6−8), 1815−1825.
(37) Cagnol, F., et al. Humidity-controlled mesostructuration in CTAB-templated silica thin film processing. The existence of a modulable steady state. *J. Mater. Chem.* **2003**, *13* (1), 61−66.
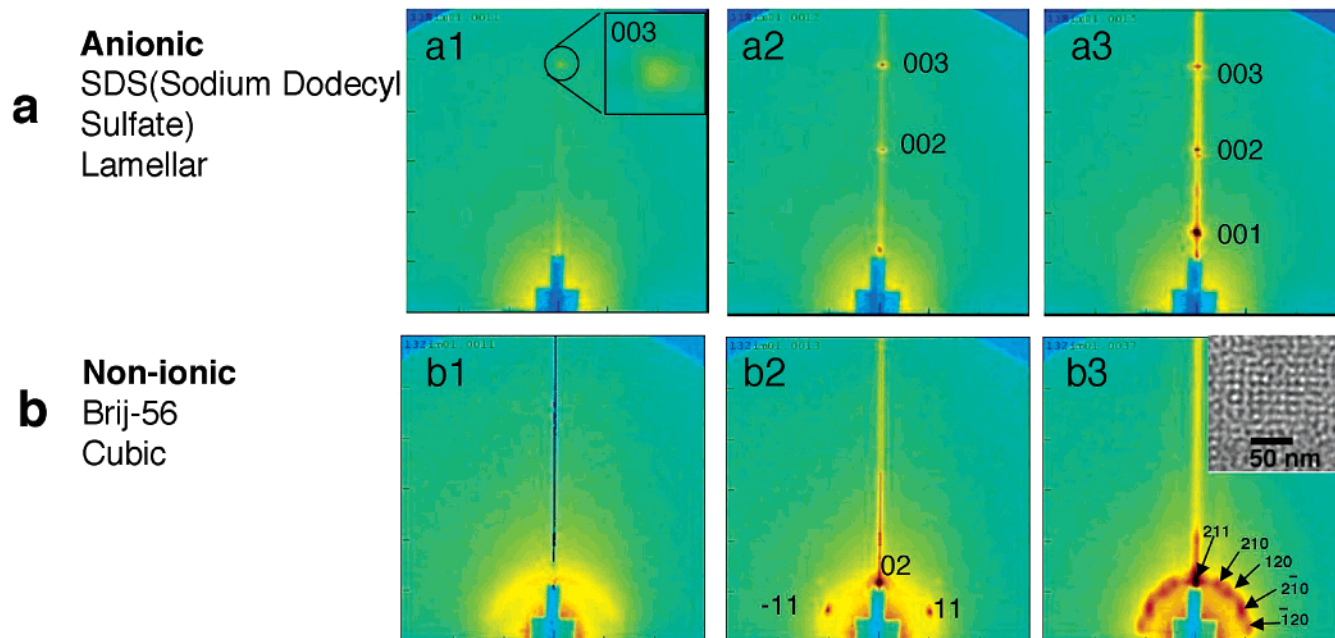
Figure 9. In situ structural evolution of lamellar and cubic mesophases probed by GISAXS. (a) Film prepared with the anionic surfactant SDS results in a lamellar phase. (b) Film prepared with Brij-56 (B56) results in a cubic phase b3 through a hexagonal intermediate b2. Inset: TEM image of the [100] orientation of the cubic mesophase.

Table 1. Changes in the Hexagonal Unit Cell Parameters during EISA for Three Different CTAB/Si Samples

CTAB/Si	$a_{fcr}(wet)^a$ Å	$c_{fcr}(wet)^a$ Å	$a_{fcr}(dry)^b$ Å	$c_{fcr}(dry)^b$ Å	% Δa_{fcr}
0.10	49.7	88.2	50.0	71.4	0.6
0.12	46.1	80.4	51.1	74.4	10.8
0.16	41.2	72.9	48.1	77.5	16.7

^{a} (wet) refers to the point when the hexagonal phase first forms during EISA. ^{b} (dry) refers to the final dried film.
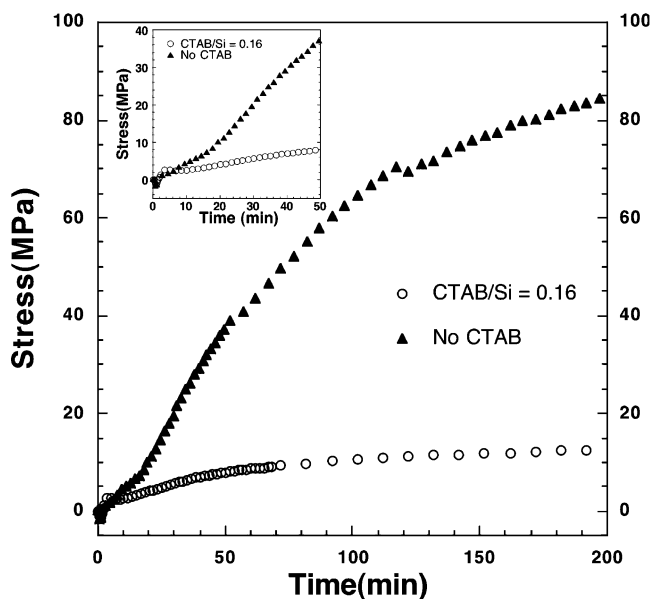
Figure 10. Cantilever beam-based stress measurements determined in situ during evaporative drying of the 0.16 CTAB/Si sol and the corresponding sol prepared without surfactant. Inset: first 50 min of stress development.

and for the corresponding sample prepared without CTAB. Both samples were maintained in a horizontal configuration with approximately the same drying conditions as those for GISAXS

and stress measurements. Comparison of the envelopes of absorption bands associated with longitudinal optical (LO) and transverse optical (TO) asymmetric stretching modes of Si–O–Si bonds 1000–1250 cm^{-1} [38–40] shows a progressive increase in absorbance with time for both samples due to the increasing concentration of oligosilicic acid species that results from solvent evaporation along with any additional siloxane condensation reactions. The differing rates of increase reflect principally the lower evaporation rate of the CTAB-containing sample (as confirmed by gravimetry). We also note a significant broadening of the absorbance envelope at longer times for the CTAB-containing sample. Using the assignments of Fidalgo[38] (red-shifted by 20 cm^{-1} to account for a lower extent of condensation), we decomposed this envelope into four Gaussians centered at 1051, 1070, 1126, and 1168 cm^{-1} [38] and determined their temporal behaviors. As shown in Figure 12, the broadening of the absorbance envelope for the CTAB sample is accounted for by the development of an absorbance band centered at 1168 cm^{-1} over the approximate time span 400–700 s. As the shape of this curve differs from that expected simply from the increasing concentration of siloxane bonds due to solvent evaporation (observed for the sample prepared without CTAB), we attribute the enhanced 1168-cm^{-1} absorbance (at least in part) to other factors such as the formation of additional siloxane bonds or perhaps siloxane bond orientation. One possibility consistent with a recent FTIR study by Innocenzi et al.[40] is the assignment of the 1168-cm^{-1} band to the LO mode of a cyclic tetrasiloxane (four-membered ring), the larger absorbance of this band indicating that four-membered ring formation is favored

(38) Fidalgo, A.; Ilharco, L. M. The defect structure of sol–gel-derived silica/polytetrahydrofuran hybrid films by FTIR. *J. Non-Cryst. Solids* **2001**, *283* (1–3), 144–154.

(39) Innocenzi, P. Infrared spectroscopy of sol–gel derived silica-based films: a spectra-microstructure overview. *J. Non-Cryst. Solids* **2003**, *316* (2–3), 309–319.

(40) Innocenzi, P., et al. Order–disorder transitions and evolution of silica structure in self-assembled mesostructured silica films studied through FTIR spectroscopy. *J. Phys. Chem. B* **2003**, *107* (20), 4711–4717.
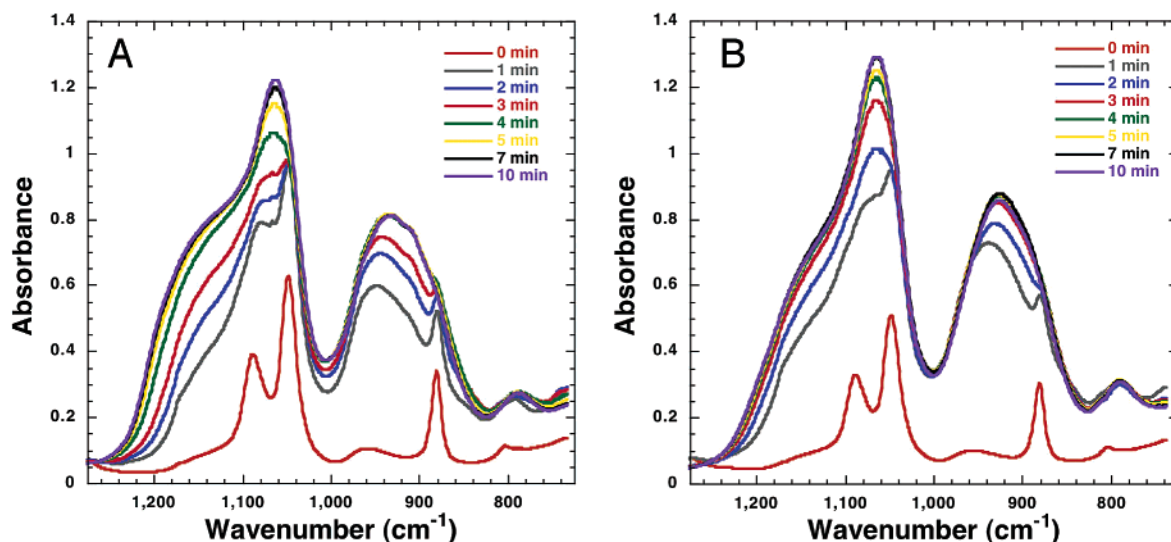
Figure 11. Attenuated total reflection FTIR spectra acquired in situ during drying (A) the 0.16 CTAB/Si sol and (B) the corresponding sol prepared without surfactant as for Figure 10.
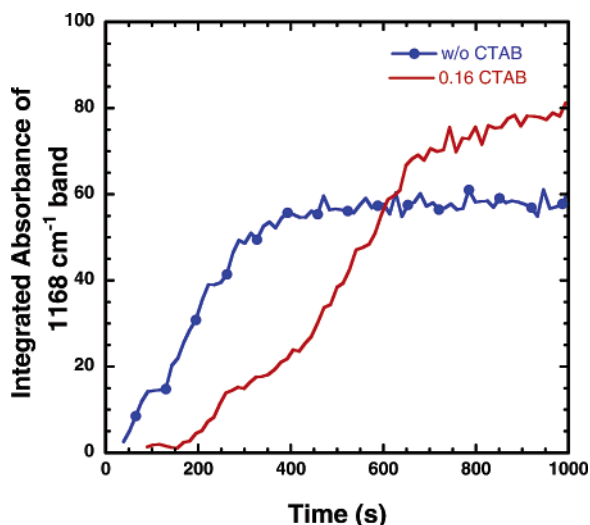

Figure 12. Temporal evolution of the integrated absorbance of the 1168 cm^{-1} Gaussian peak obtained from spectra in Figure 11 for the 0.16 CTAB/Si sol and the corresponding sol prepared without surfactant.

for surfactant templated vis-à-vis nontemplated silica. Conceivably, the condensation reaction of silanols to form siloxane bonds, when confined within the uniform ~2-nm thick walls of the silicatropic mesophase, forms principally four-membered rings as opposed to larger five- and six-membered rings that are the most common ring sizes found in conventional amorphous silica as well as high surface area silica gels dried at room temperature.[41] In support of this hypothesis, Raman spectra obtained for hexagonal thin-film mesophases formed from the identical sol using a nonionic (Brij56) surfactant show only a 490-cm^{-1} band in the spectral region 300−500 cm^{-1} associated with oxygen ring-breathing modes, along with a pronounced 1173-cm^{-1} shoulder in the IR (we are unable to obtain Raman spectra for the CTAB samples due to fluorescence). Both MD simulations[42,43] and model compound studies have attributed

the 490-cm^{-1} band to the symmetric oxygen ring breathing mode of four-membered rings. For the CTAB sample, Figure 12 shows the greatest increase in absorbance of the 1168-cm^{-1} band to occur in the time range 400−700 s, where GISAXS shows the development of mesostructural order (Figure 2), strengthening the argument that four-membered rings form preferentially due to the interfacially mediated organization of the silicic acid constituents within the uniform 2-nm thick walls of the hexagonal mesophase. This confined geometry may impose physical constraints that serve to limit the distribution of siloxane bond angles and their orientations, favoring the formation of cyclic tetrasiloxanes. Additionally, as was shown for base-catalyzed systems,[44] the complementary geometries of the four-membered ring and the CTAB headgroup should facilitate multidentate coordination, causing four-membered rings to be preferred to monomeric and smaller oligomeric silicate species.[44] In comparison to the CTAB-containing sample, Figure 12 shows the temporal evolution of the 1168-cm^{-1} band for the sample without CTAB to vary as expected for the concentration of four-membered rings as a result of solvent evaporation. It is interesting to note the near absence of four-membered rings in the CTAB-containing film in the initial stages of evaporation. This may indicate that hydrogen-bonding interactions with CTAB in the acid-catalyzed sol actually inhibit four-membered ring formation compared to the corresponding sol prepared without CTAB.

Closing Comments

GISAXS combined with gravimetry, stress analysis, and ATR-FTIR represents a general, comprehensive approach to study evaporation-induced self-assembly (EISA) in situ. Our complete elucidation of the self-assembly process has established for the first time composition/structure relationships needed to understand it and ultimately control or manipulate it so as to tailor the properties of the resultant thin-film nanostructures. For example, we now recognize the opportunity to controllably

(41) Brinker, C. J.; Scherer, G. W. *Sol−Gel Science*; Academic Press: San Diego, 1990; pp 139−142.
(42) Garofalini, S. H.; Martin, G. Molecular Simulations of the Polymerization of Silicic-Acid Molecules and Network Formation. *J. Phys. Chem.* **1994**, *98* (4), 1311−1316.
(43) Martin, G. E.; Garofalini, S. H. Sol−Gel Polymerization − Analysis of Molecular Mechanisms and the Effect of Hydrogen. *J. Non-Cryst. Solids* **1994**, *171* (1), 68−79.
(44) Firouzi, A., et al. Alkaline lyotropic silicate-surfactant liquid crystals. *J. Am. Chem. Soc.* **1997**, *119* (15), 3596−3610.

interrupt EISA to derive novel intermediate sandwichlike structures (e.g., Figure 8) or fine-tune the *d*-spacing and associated properties such as surface area, refractive index, and dielectric constant. Concerning the general topic of self-assembly of silica/surfactant mesophases, it is well recognized that for systems involving strong electrostatic interactions, for example, anionic silicate/cationic surfactant self-assembly that occurs with CTAB under basic conditions, multidentate bonding of silicate anions can screen electrostatic headgroup interactions, reducing the optimal headgroup area and local aggregate curvature.[44] This alters the self-assembly pathway causing silica/surfactant mesophases often to be different from those of the corresponding water/surfactant mesophases. Conversely, under conditions where electrostatic interactions are weak, such as the acidic conditions studied here (where the silicate oligomers are weakly charged), Attard et al.[45] showed the silicate/surfactant mesophase to be identical to the corresponding water/surfactant mesophase. Therefore, the differences between systems prepared with and without silicate observed by us for evaporation-induced silica/surfactant self-assembly (e.g., Figures 3−5) are mainly attributable to interfacial (observance of a lamellar intermediate) and kinetic effects. In particular, we must emphasize the role of silicic acid in promoting, rather than retarding, self-assembly. Oligosilicic acids apparently serve as nonvolatile hydrophilic fluids that replace water at the final stage of EISA. If they remain

weakly condensed, as we show for acidic conditions (note the absence of stress development in Figure 10), they allow self-assembly to proceed unimpeded.

JA0295523

(45) Attard, G. S.; Glyde, J. C.; Goltner, C. G. Liquid-Crystalline Phases as Templates for the Synthesis of Mesoporous Silica. *Nature* **1995**, *378* (6555), 366−368.